FAST FAULT RECOVERY SCENARIOS FOR THE JAEA-ADS LINAC*

B. Yee-Rendon†, J. Tamura, Y. Kondo, K. Nakano, H. Takei, F. Maekawa and S. Meigo
Japan Atomic Energy Agency (JAEA), Tokai, Japan

Abstract

Japan Atomic Energy Agency (JAEA) is designing a 30 MW CW superconducting proton linac as a major component for the accelerator-driven subcritical system (ADS) project. The main challenge of the linac operation is the high reliability required to avoid thermal stress in the reactor. To this end, we implemented fault compensation schemes to enable a fast beam recovery; consequently, reducing the beam trip duration. This work presents strategies to increase the fault-tolerance capacity of the JAEA-ADS linac.

INTRODUCTION

The Japan Atomic Energy Agency (JAEA) is designing an accelerator-driven subcritical system (ADS) that employs a 30 MW CW proton accelerator for the transmutation of the minor actinides [1]. Table 1 summarizes the most relevant parameters of linear accelerator (linac). Among all the specifications, reliability is the most stringent requirement; thus, the JAEA-ADS Superconducting Radio-Frequency (SRF) linac is designed to be a reliability-oriented accelerator [3].

Table 1: Main Characteristics of the JAEA-ADS Accelerator

Parameter		Beam trip duration
Particle	Proton	
Beam current (mA)	20	
Beam energy (GeV)	1.5	
Duty factor (%)	100 (cw)	
Frequency (MHz)	162/ 324/ 648	
Beam loss (W/m)	< 1	
Beam trips per year [2]	2×10^4	≤ 10 s
	2×10^3	from 10 s to 5 min
	42	>5 min
Length (m)	429	

To achieve a reliability-oriented goal, we started by developing a strong lattice design that has a simple configuration, strict control of beam loss, and operates with de-rated SRF cavities. Additionally, we optimized the number of cavities and the linac length to reduce the operational cost. Figure 1 shows the schematic configuration of the linac. The main linac has three different types of SRF cavities operating at different frequencies: Half-Wave Resonator (HWR) operates at 162 MHz, Single Spoke Resonator (SSR), at 324 MHz, and five-cell Elliptical Resonator (EllipR), at 648 MHz. Additionally, the three SRF cavities are grouped into five sections, as is shown in Fig. 1. Table 2 describes the SRF configuration periods using the following notation: C= SRF cavity, S= solenoid, DQ= doublet quadrupole.

Table 2: Lattice Configuration in the Main Linac

Section	Layout	Length (m)	Periods
HWR	S-C	0.7	25
SRR1	S-C^2	1.7	33
SSR2	S-C^3	3.4	24
EllipR1	DQ-C^3	5.7	20
EllipR2	DQ-C^5	9.9	14

After obtaining a robust beam optics design [4, 5], the following step is to ensure a linac operation below the limits of the beam trips to avoid thermal fatigue in the reactor components, Table 1. To this end, we pursued the ability to operate the accelerator with an acceptable beam performance in the presence of undesired behavior of machine components, the so-called Fault-tolerance [3]. This work investigated the Fault-Tolerance Compensation Scheme (FTCS) for SRF cavity or magnet failures reduce the system downtime; consequently, the accelerator reaches the reliability requirements for the JAEA-ADS machine.

FAULT-TOLERANCE

Fault-tolerance is accomplished by using parallel and serial redundancy. Parallel redundancy duplicates partially or completely the linac. In the case of full duplication linac, both linacs operate independently. On the contrary, one is used as the main accelerator and the other as hot-spare. For the serial redundancy, this approach exploits the linac's modularity by using the none Faulty-element to compensate for the unwanted effect of the Faulty-element. JAEA-ADS linac employs a combined strategy of parallel redundancy at the low-energy part and serial redundancy for the high-energy part. The general plan for the FTCS consists of the following steps:

- Fast detection of an abnormal element, SRF cavity or magnet, behavior.
- Fast Faulty-element detuning.
- Beam operation is stopped.
- Pre-calculated compensation settings are uploaded.
- Beam operation is resumed.

The entire process must take few seconds to increase the number of acceptable beam trips. Thus, we focused on local schemes, i.e., using neighboring elements to compensate for a fast beam operation recovery [6–8]. Figure 2 illustrates the Faulty-SRF cavity compensation scheme; nevertheless, the Faulty-magnet one is the same. The settings of the none Faulty-elements were re-adjusted to recovery beam conditions similar to the baseline operation. We mainly use the

* Work supported by Subvention for ADS development.
† byee@post.j-parc.jp

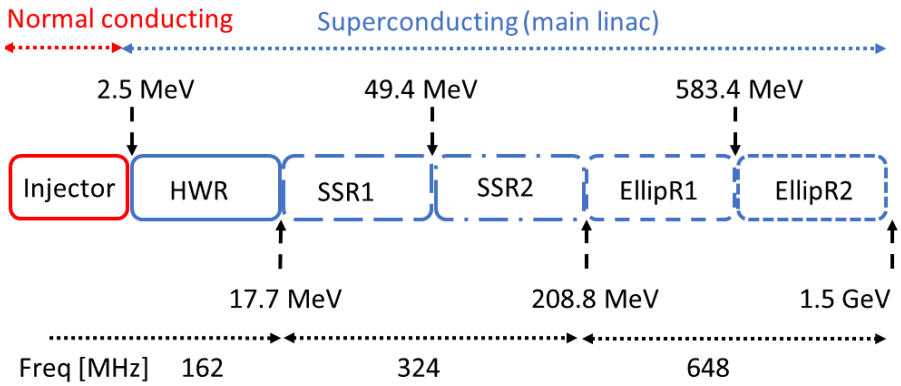

Figure 1: Linac lattice configuration.

same type of element to compensate, and the other type improves the matching and emittance. For a Faulty-SRF cavity, the cavities restitute the missing energy, and the magnets help to recovery beam values at a certain point downstream of the failure location.

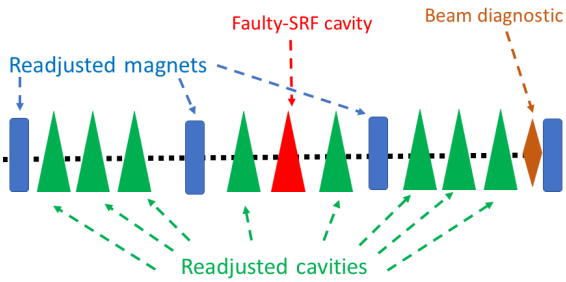

Figure 2: FTCS for SRF cavities.

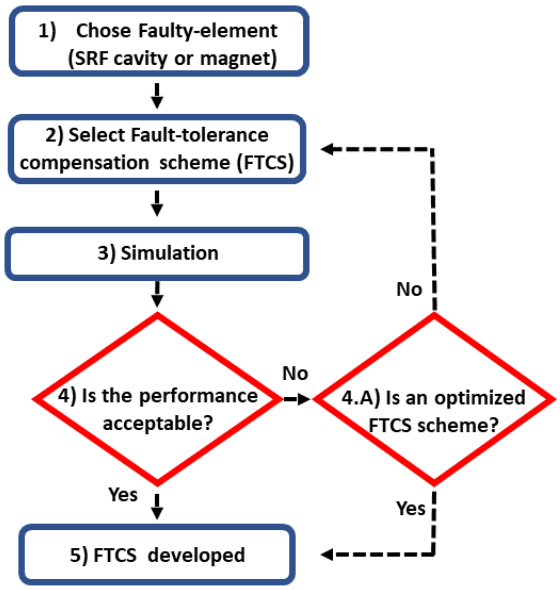

Figure 3: Flowchart of the FTCS in TraceWin.

To decide until which energy we can successfully use serial redundancy, FTCSs were developed using the TraceWin program [9], and the flowchart for its implementation is presented in Fig. 3. In the selection of the FTCSs, we minimize the number of readjusted elements to reduce the complexity. In addition, we included restraints in the maximum variation of readjusted parameters; for example, the maximum electric peak (E_{pk}) inside the SRF cavities was 36 MV/m. The FTCSs were evaluated using multiparticle simulations in two steps. First, the scheme was tracking within few periods before and after the Faulty-element for fast selection of possible FTCSs. Then, the candidate scheme was simulated until the end of the linac to estimate the error propagation. The selection criteria for local and global multiparticle tracking were the absence of new beam lost and achieved similar beam performance as the baseline model. The last criterion refers that the difference in the final energy ($\Delta E/E_0$) should be lower than 1%, the emittance growth on the transverse plane ($(\Delta\epsilon/\epsilon_0)_t$) does not increase the double, and the mismatch (M) lower than 0.2.

SRF Cavities

The main linac is composed of 293 SRF cavities; thus, the testing for each element will require a considerable amount of time. Therefore, instead of analyzed all the SRF cavities, we studied the cavities and the beginning, middle, and end cryomodules of the five different sections. As an example, Fig. 4 shows the FTCS when the last cavity of EllipR1 was set down. In this case, the four upstream and the three downstream cavities were used to compensate. Figure 4-top and middle shows the readjusted in synchronous phase (ϕ_s) and accelerating gradients (E_{acc}), respectively. Subsequently, the energy compensation is observed in Fig. 4-bottom.

In almost all the main linac, the implemented FTCSs produced satisfactory results; however, the HWR FTCS recorded beam loss and significant beam degradation. Thus, we decide to apply the FTCS from SSR1 to the end of the linac. Table 3 provides a summary of the worst performance for each of the different SRF cavity sections. The emittance growth was lower than 36% for all the cases, M was below

0.13, $\Delta E/E_0$ is lower than 0.02%, and the constraint in the E_{pk} was kept.

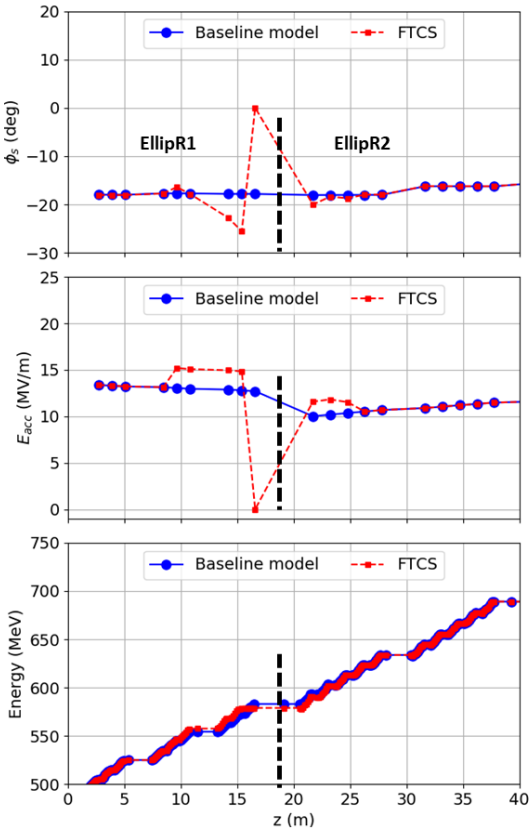

Figure 4: FTCS for the failure in the last EllipR1's cavity. The black dotted vertical line indicates the transition between EllipR1 and EllipR2 regions.

Table 3: Summary of the Beams Optics Performance for the Worst SRF Cavity's FTCS

Parameters	SSR1	SSR2	EllipR1	EllipR2
$(\Delta\epsilon/\epsilon_0)_t$ (%)	12.2	1.9	3.5	0.4
$(\Delta\epsilon/\epsilon_0)_l$ (%)	35.8	7.8	4.5	1.4
M_t	0.03	0.06	0.03	0.04
M_l	0.06	0.04	0.09	0.12
$\Delta E/E_0$ (%)	0.00	0.01	0.01	0.00
Max E_{pk}(MV/m)	32.6	35.9	35.4	35.9
Max B_{pk}(mT)	48.3	51.9	66.1	69.3

Additionally, we investigate the scenarios of several Faulty-SRF cavities that occurred at the same time. To this end, we investigated two cases: multiples Faulty-SRF cavities (MSRFC) in independent cryomodules and a full Faulty-cryomodule (FCRYO). For the MSRFC case, the initial SRF cavity of each section, from SSR1 to EllipR2, was set down. In addition, the final cavity of EllipR2, the last one of the linac, was also simulated as a Faulty-cavity. Figure 5 shows the ϕ_s and E_{acc} for the Baseline model and the FTCS one. The location of the five Faulty-SRF cavities corresponds to the points where ϕ_s and E_{acc} are zero. We compensated these failures using the scheme developed above for a single Faulty-SRF cavity, and the result is summarized in Table 4. The overall beam performance is acceptable, despite the increase of 50% in the longitudinal emittance that does not represent a potential threat.

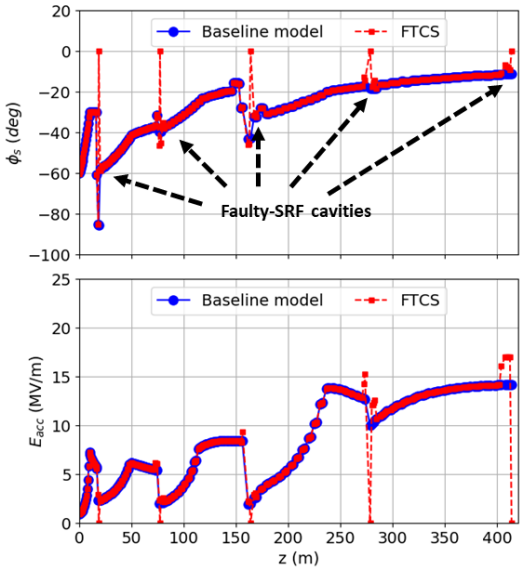

Figure 5: ϕ_s (top) and E_{acc} (bottom) plots for multiples SRF cavity failures along the linac.

Table 4: Summary of the Beams Optics Performance for the Multiples Faulty-SRF Cavities (MSRFC) and Full Faulty-cryomodule (FCRYO)

Parameters	MSRFC	FCRYO
$(\Delta\epsilon/\epsilon_0)_t$ (%)	9.2	1.3
$(\Delta\epsilon/\epsilon_0)_l$ (%)	50	-2.5
M_t	0.04	0.16
M_l	0.16	0.64
$\Delta E/E_0$ (%)	0.01	0.03
Max E_{pk}(MV/m)	35.9	35.9
Max B_{pk}(mT)	69.3	69.3

In the FCRYO case, we have chosen the failure of the last cryomodule of EllipR2 because it is the most challenging in terms of energy compensation, about 72 MeV. The FTCS model required the five periods upstream of the Faulty-cryomodule, as shown in Fig. 6. The main difference with the previous cases is the change in phase for the readjusted SRF cavities. For the above cases, the ϕ_s adjusted was slight because the energy difference between the baseline and FTCS was relatively small; however, for this case, the energy difference is appreciable. Therefore, we pre-calculated the new ϕ_s and made the adjusting cavity by cavity to avoid a considerable reduction of the phase acceptance. Figure 6-top shows the ϕ_s phase was not significantly changed; thus, the

phase acceptance was basically preserved. Table 4 presents that the beam performance for the FCRYO fulfills the goal criteria.

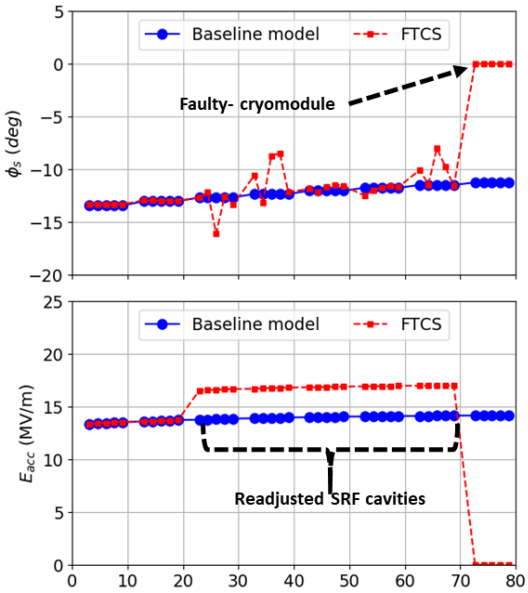

Figure 6: ϕ_s (top) and E_{acc} (bottom) plots for the failure of the last cryomodule of the linac.

Magnets

The last case that we investigate was failures in magnets. JAEA-ADS linac has 83 solenoids and 35 doublet quadrupoles, i.e., 70 normal quadrupoles. We started using only magnets to compensate for the transverse focusing and cavity for the matching. This strategy works well for double quadrupoles; however, for solenoids, the control of the beam envelopes was not enough resulting in beam loss. Thus, SRF cavities were used to recover the transverse focusing [10].

Figure 7 shows the change on the solenoid's magnetic field (top) and the SRF cavity's ϕ_s (bottom) for a failure is the first solenoid of SSR2. For this case, three upstream and four downstream periods magnets were required. The readjusted SRF cavities were in one period upstream and on the same period of the Faulty-magnet. For the same failure, the maximum horizontal envelope until the end of the linac is presented in Fig. 8. The region plotted corresponds from the last period of SSR1, about 70 m from the main linac's entrance, until the end of the linac. For the FTCS case using only magnets for compensating the transverse focusing (green dotted dashed), the envelope reached the aperture; consequently, beam loss appeared. When the FTCS employed magnets and SRF cavities (blue dotted line), the envelope growths are controlled, and a similar evolution as the baseline (red dashed) is achieved.

Table 5 provides a summary of the worst cases for each of the SRF sections. Similar to the Faulty-SRF cavities, FTCS provided an acceptable beam performance from the SSR1 to the end of the linac. At HWR, beam envelopes became large even with the use of SRF cavities; consequently, beam

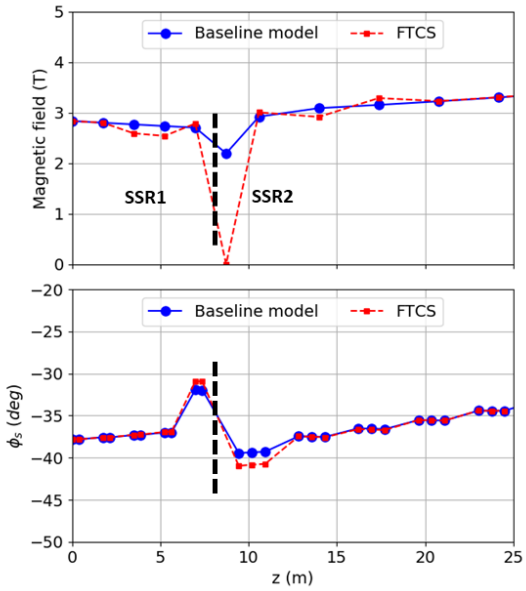

Figure 7: FTCS for the failure in the first SSR2 solenoid. The black dotted vertical line indicates the transition between SSR1 and SSR2 regions.

loss appeared. It is worth mentioning that the worst case for each section corresponds to the first-period magnet, except for the EllipR2 that whose worst case was the failure in the last period.

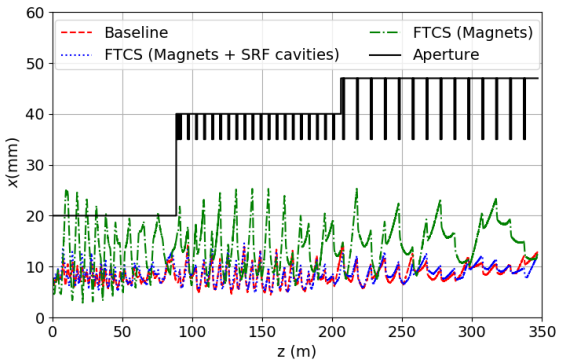

Figure 8: Horizontal beam envelope for different models. The start point begins from the last five periods of SSR1 until the end of the linac.

Table 5: Summary of the Beams Optics Performance for the Worst Magnet Compensation Case in Each Section

Parameters	**SSR1**	**SSR2**	**EllipR1**	**EllipR2**
$(\Delta\epsilon/\epsilon_0)_t$ (%)	63.7	8.2	22.1	35.8
$(\Delta\epsilon/\epsilon_0)_l$ (%)	63.1	10.1	4.6	7.5
M_t	0.08	0.04	0.06	0.12
M_l	0.17	0.04	0.03	0.16
$\Delta E/E_0$ (%)	-0.04	-0.01	0.01	0.00

CONCLUSIONS

The Fault-tolerance studies demonstrated serial redundancy capabilities from the SSR1 section until the end linac without a severe beam degradation. In addition, it showed that the linac could operate in the presence of multiples Faulty-SRF cavities and even in the case of a full cryomodule failure. Thus, it shows the possibility of fast recovery after a failure of a principal component: cavity or magnet. Nevertheless, the main limitation comes from the engineering side to guaranty the effectiveness of the compensation. We need to reduce the time required to trusty detect an abnormal element behavior, detune the element, and applied the compensation setting. To this end, we require a large R&D effort to overcome these difficulties.

ACKNOWLEDGMENTS

The authors would like to thank to the members of the JAEA-ADS and J-PARC linac groups for their comments and suggestions.

REFERENCES

[1] K. Tsujimoto *et al.*, "Neutronics design for lead-bismuth cooled accelerator-driven system for transmutation of minor actinide", *JNST*, vol. 41, no. 21, p. 21, Jan. 2004. doi:10.1080/18811248.2004.9715454

[2] H. Takei, K. Nishihara, K. Tsujimoto, and H. Oigawa, "Estimation of acceptable beam-trip frequencies of accelerators for accelerator- driven systems and comparison with existing performance data", *J. Nucl. Sci. Techol.*, vol. 49, p. 384, Sep. 2012. doi:10.1088/00223131.2012.669239

[3] J.L. Biarrotte, "Reliability and fault tolerance in the European ADS project", CERN, Geneva, Switzerland, Rep. CERN-2013-001.481, Jun. 2011.

[4] B. Yee-Rendon, Y. Kondo, F. Maekawa, S. Meigo, and J. Tamura, "Beam optics design of the superconducting region of the JAEA ADS ",*J. Phys. Conf. Ser.*, vol. 1350, p. 12120, Sep. 2019. doi:10.1088/1742-6596/1350/1/012120

[5] B. Yee-Rendon *et al.*, "Present Status of the R&D of the Superconducting Linac for the JAEA- ADS", *J. Phys. Soc. Jpn.*, vol. 33, p. 011043, March 2021. doi:10.7566/JPSCP.33.011043

[6] J.-L. Biarrotte, M. Novati, P. Pierini, H. Safa, and D. Uriot, "Beam Dynamics Studies for the Fault Tolerance Assessment of the PDS-XADS Linac Design",in *Proc. 9th European Particle Accelerator Conf. (EPAC'04)*, Lucerne, Switzerland, Jul. 2004, paper TUPLT057, pp. 1282–1284.

[7] F. Bouly, J.-L. Biarrotte, and D. Uriot, "Fault Tolerance and Consequences in the MYRRHA Superconducting Linac ",in *Proc. 27th Linear Accelerator Conf. (LINAC'14)*, Geneva, Switzerland, Aug.-Sep. 2014, paper MOPP103, pp. 297–299.

[8] B. Yee-Rendon *et al.*, "Progress on SRF Linac Development for the Accelerator-Driven Subcritical System at JAEA ",in *Proc. 20th International Conf. on RF Superconductivity (SRF'21)* (To be published).

[9] TraceWin Manual, http://irfu.cea.fr/dacm/logiciels

[10] B. Sun J.Y. Tang, F. Yan, Z.H. Li and Cai Meng, "Local compensation–rematch for major element failures in superconducting linacs with very high reliability and low beam loss", *Nucl. Instrum. Methods Phys. Res. A.*, vol. 785, p. 77, 2015. doi:10.1016/j.nima.2015.02.051